Spin Superstructure and Noncoplanar Ordering in Metallic Pyrochlore Magnets with Degenerate Orbitals

Gia-Wei Chern[1] and Cristian D. Batista[2]

[1]*Department of Physics, University of Wisconsin, Madison, Wisconsin 53706, USA*
[2]*Theoretical Division, Los Alamos National Laboratory, Los Alamos, New Mexico 87545, USA*

(Received 17 August 2011; published 25 October 2011)

We study double-exchange models with itinerant t_{2g} electrons in spinel and pyrochlore crystals. In both cases the localized spins form a network of corner-sharing tetrahedra. We show that the strong directional dependence of t_{2g} orbitals leads to unusual Fermi surfaces that induce spin superstructures and noncoplanar orderings for a weak coupling between itinerant electrons and localized spins. Implications of our results to ZnV_2O_4 and $Cd_2Os_2O_7$ are also discussed.

DOI: 10.1103/PhysRevLett.107.186403 PACS numbers: 71.20.Be, 71.10.Fd, 75.25.Dk

Orbital degrees of freedom have attracted much attention due to their crucial role in the stability of many unusual phases of correlated materials [1]. In particular, the presence of degenerate orbitals in frustrated magnets can lift the spin degeneracy through various spin-orbital interactions. For Mott insulators with spins residing on a frustrated lattice, such as triangular or pyrochlore, geometrical constraints prevent spins from reaching a simple Néel order. The occurrence of long-range orbital order due to either Jahn-Teller distortion or orbital exchange reduces the magnetic frustration by creating disparities between nearest-neighbor (NN) exchange constants and paves the way for magnetic ordering [2,3].

However, some of the magnetic orders observed in geometrically frustrated compounds are difficult to explain starting from the strongly coupled Mott-insulator regime. For example, several vanadium spinels [4–6] exhibit a complicated magnetic structure with $\uparrow\uparrow\downarrow\downarrow\cdots$ collinear ordering along certain chains that is very puzzling from the viewpoint of localized spin models. Below, we shall provide a simple explanation for the observed spin superstructures based on a double-exchange (DE) model which takes into account orbital degeneracy. The DE model arises naturally for multiband compounds in which a narrow band of localized electrons coexists with a wider band of itinerant electrons. It can also be viewed as a mean-field approximation to the Hubbard Hamiltonian. A well-studied case is the DE model with itinerant e_g electrons on the cubic lattice [7]. This model has been shown to describe the rich physics of colossal magnetoresistance in perovskite manganites [8].

Recently, there has been tremendous interest in DE models on frustrated lattices [9–16]. The Fermi surface geometry plays a crucial role [11,16] in the nonlocal effective spin-spin interaction that results from integrating out the itinerant electrons in the weak-coupling regime. The magnetic structures stabilized by itinerant electrons are thus often difficult to understand by using short-range spin models. For example, an unusual noncoplanar magnetic order, in which spins on different sublattices point toward the corners of a tetrahedron, is shown to appear in different coupling regimes and various commensurate filling fractions on the triangular lattice [11–14]. Recent investigations of DE models on pyrochlore lattice also reveal interesting behaviors such as electronic phase separation [15] and a complex noncoplanar order [16] at quarter filling. However, most of these studies ignore the orbital dependence and consider only isotropic electron hopping.

In this Letter, we examine DE models with itinerant t_{2g} electrons in both spinel and pyrochlore structures with general formulas AB_2O_4 and $A_2B_2O_7$, respectively. In addition to the itinerant electrons, there are localized magnetic moments residing on the B sites of the crystal which form a 3D network of corner-sharing tetrahedra. These moments are approximated by classical vectors under the assumption that the ferromagnetic nature of Hund's coupling does not lead to strong quantum fluctuations. The O_6 octahedron surrounding the B sites creates a cubic crystal field which splits the d levels into the e_g doublet and the lower-energy t_{2g} triplet. The strong dependence of electron hopping on orbital orientation leads to peculiar Fermi surfaces in both cases. In particular, the electron subsystem reduces to a set of cross-linking Kondo chains in spinels. We show that this feature leads to a weak-coupling instability towards the previously mentioned $\uparrow\uparrow\downarrow\downarrow$ superstructure in vanadium spinels. Fermi surface nesting of different origin leads to noncoplanar all-in–all-out magnetic order in pyrochlores, which is a candidate state for the intermediate insulating phase of $Cd_2Os_2O_7$.

Frustrated Kondo chains in spinels.—In the spinel structure, a common quantization axis can be defined for t_{2g} electrons at all crystal B sites [Fig. 1(a)]. The shape of the t_{2g} orbitals is such that the strongest overlap is between the same orbitals along a particular NN direction, e.g., between two d_{xy} orbitals along either a [110] or $[1\bar{1}0]$ bond in the xy plane. Keeping only this dominant term, electrons

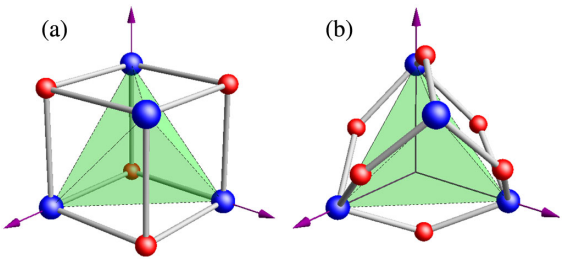

FIG. 1 (color online). A unit cell of the pyrochlore lattice and the configuration of local oxygen octahedra in (a) spinel and (b) pyrochlore crystals. The blue and red balls denote the (B-site) transition-metal and oxygen ions, respectively.

in a given orbital state can only hop along the corresponding $\langle 110\rangle$ chain on the pyrochlore lattice. We thus divide these chains into three types: yz, zx, and xy, depending on the active orbitals along the chain. Since the kinetic energy preserves the orbital flavor, the Hamiltonian is a sum of contributions from different orbital sectors: $\bar{H} = \sum_m H_m$, where

$$H_m = -t \sum_{\langle ij\rangle \| m} (c^\dagger_{im\alpha} c_{jm\alpha} + \text{H.c.}) - \tilde{J}_H \sum_i \mathbf{S}_i \cdot \mathbf{s}_{im}, \quad (1)$$

$m = xy, yz, zx$, and $\mathbf{s}_{im} = \frac{1}{2}\sum_{\alpha\beta} c^\dagger_{im\alpha} \boldsymbol{\sigma}_{\alpha\beta} c_{im\beta}$. Here the first term describes NN hopping of t_{2g} electrons along a $\langle 110\rangle$ chain of type m; t is the dominating $dd\sigma$ transfer integral. $c^\dagger_{im\alpha}$ is the creation operator for d electrons at site i with orbital flavor $m = xy, yz, zx$ and spin $\alpha = \uparrow, \downarrow$. The second term in Eq. (1) describes an effective on-site Hund's coupling between t_{2g} electrons and localized classical spins $\mathbf{S}_i$ (with normalization $|\mathbf{S}_i| = 1$). By regarding model (1) as a mean-field approximation for a three-band Hubbard Hamiltonian that has the same kinetic energy term as $\bar{H}$, the effective coupling constant is $\tilde{J}_H = 4(U/9 + 4J_H/9)|\langle \mathbf{s}_i\rangle|$, where $U + J_H$ is the Coulomb repulsion between two electrons in the same orbital and J_H is the bare Hund's coupling [17].

$\bar{H}$ models a collection of ferromagnetic Kondo chains coupled together by the local moments. While a classical Kondo chain is a relatively simple system, the fact that each spin is shared by three chains with different orbitals introduces geometric frustration. Numerical methods such as Monte Carlo calculations become very inefficient for conventional 3D DE models, because the dimension of the electron Hamiltonian to be diagonalized for each spin update scales as $L^3 \times L^3$ for systems with linear size L. On the contrary, for $\bar{H}$, one needs only to diagonalize matrices whose dimension scales as $L \times L$ for the three Kondo chains intersecting at the updated spin. The reduced dimensionality of the problem thus allows for studying the ground states of $\bar{H}$ with the aid of unbiased large-scale Monte Carlo simulations.

We first consider the case with three d electrons per site. The electron energy is minimized by placing one electron at each of the three different 1D bands, giving rise to half filled Kondo chains with a Fermi wave vector $k_F = \pi/2l$ [Fig. 2(c)], where l is the NN distance. The two Fermi points are nested by a commensurate wave vector $q_{1/2} = 2k_F = \pi/l$, leading to magnetic Néel order in the presence of Hund's coupling. However, direct inspection shows that such a collinear Néel order cannot be simultaneously attained on all chains of the pyrochlore lattice. Instead, Monte Carlo simulations on $L = 8$ lattices (with $16L^3$ spins) show that the total energy is minimized by the noncoplanar all-in–all-out spin order shown in Fig. 2(a). The magnetic order of each chain consists of ferromagnetic and staggered components, which are perpendicular to each other. A similar noncoplanar structure also occurs in pyrochlore compounds, e.g., $Ho_2Ti_2O_7$, generally known as spin ice [18]. It is worth noting that, while the noncoplanar spins in spin ice are stabilized by strong single-ion anisotropies, the DE Hamiltonian $\bar{H}$ is rotationally invariant; any global rotation of the all-in–all-out order leads to another ground state of $\bar{H}$.

The situation is more complicated for transition metals with two d electrons per site, like the vanadium spinels AV_2O_4, where A = Zn, Cd, or Mg. In an ideal cubic spinel, equal distribution of electrons among the Kondo chains corresponds to $1/3$ filling fraction. The classical ground state of a single Kondo chain at $1/3$ filling has a $\uparrow\uparrow\downarrow$ magnetic order with a period of $3l$. Again, such a simple arrangement of spins is precluded by geometric frustration. Our numerical minimization on large finite systems yields

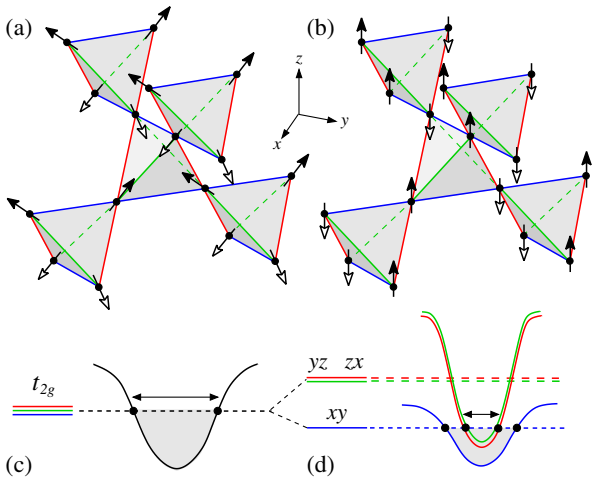

FIG. 2 (color online). (a) The noncoplanar all-in–all-out magnetic order and (b) collinear spin superstructure with wave vector $\mathbf{Q} = (0, 0, 2\pi/a)$ in spinels. Note the $\uparrow\uparrow\downarrow\downarrow\cdots$ order along yz and xz chains and a $\uparrow\downarrow\uparrow\downarrow\cdots$ Néel order on xy chains in (b). Panels (c) and (d) show the corresponding electron band structures of the three 1D chains with different orbitals. In (c) all three types of bands are half filled, leading to the noncoplanar order in (a) when perturbed by Hund's coupling. The filling fractions in (d) are $1/2$ for xy band and $1/4$ for both yz and zx bands. Inclusion of J_H gives rise to the collinear superstructure in (b).

a 3D noncoplanar magnetic order with wave vector $\mathbf{Q} = \frac{2\pi}{a}(\frac{1}{3}, \frac{1}{3}, 1)$, where $a = 2\sqrt{2}l$ is the length of a conventional cubic unit cell; the extended magnetic unit cell contains 108 spins.

Collinear superstructure in vanadium spinels.—Instead of the above complex order which preserves orbital degeneracy, experiments showed that vanadium spinels undergo a cubic-to-tetragonal structural transition with lattice constants $c < a = b$ [4–6]. Contrary to the elongation, which is favored by a Jahn-Teller ion with two t_{2g} electrons, the observed tetragonal compression can be understood as originating from the band Jahn-Teller instability. The lattice distortion results in a crystal-field splitting of the t_{2g} levels as shown schematically in Fig. 2(d). With two d electrons per site, the lower-energy xy orbital is always occupied by one electron in the intermediate and strong-coupling regimes. By assuming that the mean-field derivation of Eq. (1) can be extended into the intermediate-coupling regime, we obtain a DE Hamiltonian with $S = 1/2$ local moments provided by the electron that is localized in each xy orbital:

$$H_{\mathrm{DE}} = \sum_{m=yz,zx} H_m + J_{\mathrm{AF}} \sum_{\langle ij\rangle \| xy} \mathbf{S}_i \cdot \mathbf{S}_j. \tag{2}$$

The lattice distortion also reduces the hopping integral of xy electrons providing further justification for the derivation of Eq. (2). Here J_{AF} is the exchange constant between localized spins along the [110] and [1$\bar{1}$0] chains. As the magnet is cooled, antiferromagnetic spin correlations develop first along these chains as indeed observed [4]. A long-range 3D magnetic order resulting from interactions between different spin chains sets in at a lower temperature [4–6]. However, the crossing-chain coupling is geometrically frustrated if only NN spin interactions are taken into account [19,20].

Here we provide a simple picture of the unusual magnetic order of these vanadates based on the DE model (2). Because the other d electron can occupy either yz or zx orbitals, the corresponding bands are both 1/4 filled. In the presence of Hund's coupling J_H, the usual Fermi-point nesting thus leads to the formation of ↑↑↓↓ $\cdots$ superstructure with $q_{1/4} = 2k_F = \pi/2l$ on both yz and zx chains. In the weak-coupling regime, this collinear ordering (same amplitude for $\pm q_{1/4}$) is always more stable than the single-q spiral order, because both wave vectors $q_{1/4}$ and $-q_{1/4}$ are required to gap the two Fermi points of each chain. The corresponding 3D collinear magnetic order [Fig. 2(b)] characterized by wave vector $\mathbf{Q} = (0, 0, 1)$ is consistent with the experiments (we shall from now on express the wave vectors in units of $2\pi/a$ for convenience). This collinear structure is also free of geometrical frustration, as individual chains are in their respective ground states simultaneously. The mechanism for the formation of this magnetic order is similar to the orbitally induced Peierls instability in the spinel $MgTi_2O_4$ [21].

Although the above collinear spin order can also be explained within a local spin picture, an *ad hoc* third-neighbor antiferromagnetic exchange has to be introduced in order to stabilize the ↑↑↓↓ structure along yz and zx chains [19]. On the other hand, our approach based on the itinerant DE model provides a natural explanation for the formation of these superstructures in the absence of orbital order. In addition, recent *ab initio* calculations and experimental studies indicated that some vanadium compounds are indeed close to the metal-insulator transition [22,23], giving further support to the itinerant picture adopted here. Although the above conclusion is valid only for weak J_H/t and is based on a mean-field treatment of the multiband Hubbard model, a more exact calculation that takes into account the electron correlations gives a consistent result, which will be presented elsewhere.

Noncoplanar magnetic order in metallic pyrochlore.—We now turn to the DE model with degenerate orbitals on the pyrochlore structure [Fig. 1(b)]. Our theory provides a plausible explanation for magnetic ordering and metal-insulator transition in the pyrochlore oxide $Cd_2Os_2O_7$. This compound undergoes a continuous metal-insulator transition at $T_{\mathrm{MI}} \approx 225$ K [24–26]. The resistivity increases by 3 orders of magnitude upon cooling below T_{MI}. The transition is accompanied by a sharp reduction of magnetic susceptibility, indicating the occurrence of antiferromagnetic order [25]. The specific-heat anomaly at T_{MI} is found to be well described by a mean-field BCS-type phase transition. The electron activation energy obtained from resistivity measurements also exhibits a BCS-like behavior near T_{MI} [25].

These experimental observations justify a mean-field approach for the metal-insulator and magnetic transition in $Cd_2Os_2O_7$. As discussed above, the mean-field approximation reduces the multiband Hubbard model to the following DE model:

$$H_{\mathrm{MF}} = -\sum_{ij} \sum_{mn,\alpha} t_{ij}^{mn} c_{im\alpha}^{\dagger} c_{jn\alpha} - \tilde{J}_H \sum_i \sum_m \mathbf{S}_i \cdot \mathbf{s}_{im}. \tag{3}$$

Here the orbital index m refers to the quantization axes of the *local* crystal fields which are different in the four nonequivalent crystal B sites [Fig. 1(b)]. Contrary to the case of spinels, the orbital flavor is not conserved by the kinetic term. To obtain the hopping matrix, we expand the t_{2g} orbital wave function at a given sublattice s in the basis of common coordinates for the cubic pyrochlore: $|\phi_m^{(s)}\rangle = a_{mk}^s |\phi_k\rangle$. The details of the transformation coefficients a_{mk}^s can be found in Ref. [27]. The resulting hopping matrix is $t_{ss'}^{mn} = \sum_{kl} a_{mk}^s a_{nl}^{s'} \langle \phi_k | H_t | \phi_l \rangle$. Here the transfer integral $\langle \phi_k | H_t | \phi_l \rangle$ is expressed by using the Slater-Koster parameters [28].

We again start by considering only the dominant $dd\sigma$ hopping in the Slater-Koster parameters; the calculated tight-binding spectrum is shown in Fig. 3(a). In the metallic pyrochlore $Cd_2Os_2O_7$, the Os^{5+} ion has three d

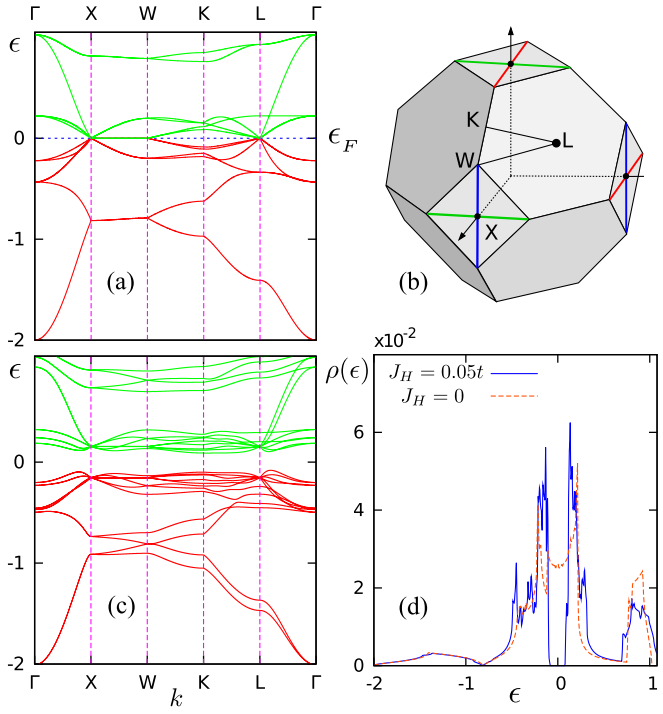

FIG. 3 (color online). (a) Band structure of the orbital-dependent tight-binding model in the pyrochlore crystal structure. At half filling, the Fermi level is at $\epsilon = 0$. (b) First Brillouin zone of the fcc lattice which is the underlying Bravais lattice of the pyrochlore crystal. The Fermi "surface" for a half filled band include three sets of Fermi lines [the XW segment in (a)] and Fermi points at the L points. (c) Band structure in the presence of nonzero Hund's constant $\tilde{J}_H = 0.05t$. (d) Calculated density of states for zero and nonzero Hund's coupling.

electrons corresponding to a half filled band. The Fermi level lies at $\epsilon = 0$ for this filling fraction, and the resultant Fermi "surface" consists of three lines and four points at the boundary of the Brillouin zone. The three Fermi lines are diagonals of the square surface at the zone boundary, while the Fermi points are located at the high symmetry L point $\mathbf{k}_{\mathrm{L}} = (\frac{1}{2}, \frac{1}{2}, \frac{1}{2})$ [Figs. 3(a) and 3(b)].

Interestingly, this unusual Fermi surface can be nested by three wave vectors: $\mathbf{Q}_1 = (1, 0, 0)$, $\mathbf{Q}_2 = (0, 1, 0)$, and $\mathbf{Q}_3 = (0, 0, 1)$. In particular, the Fermi lines are topologically equivalent to three "circles," each of which can be completely nested by one of the $\mathbf{Q}$ vectors [16]. To determine the optimal ground state, we minimize the energy among all the spin orderings for which the noninteracting system has a divergent susceptibility. In other words, we introduce a variational amplitude for the uniform ordering with $\mathbf{Q}_0 = \mathbf{0}$ and each wave vector $\mathbf{Q}_i$ that leads to perfect nesting of the Fermi surface. Restricted to this particular set of magnetic structures, our simulated-annealing minimization yields a noncoplanar spin order characterized by a single wave vector $\mathbf{Q}_0 = \mathbf{0}$; the magnetic unit cell is the same as the crystal one. Spins on the four inequivalent sites point toward the corners of a tetrahedron. The so-called all-in–all-out structure shown in Fig. 2(a) is an example of the noncoplanar "tetrahedral" order. The corresponding band structure is shown in Fig. 3(c) for Hund's coupling $\tilde{J}_H = 0.05t$. A charge gap opens at the original Fermi energy, as can also be seen in the calculated density of states [Fig. 3(d)].

The noncoplanar spin structure obtained above can be a strong candidate for the magnetic order below T_{MI} in $Cd_2Os_2O_7$. This simple $\mathbf{q} = 0$ order also preserves the cubic symmetry. Experimentally, the metal-insulator transition was found to be accompanied by a slight change in unit-cell volume of less than 0.05%. More importantly, no change in crystal symmetry was observed below T_{MI}. Although the exact magnetic structure is yet unclear, the $\mathbf{q} = 0$ noncoplanar order is consistent with a recent μSR measurement [26]. Interestingly, upon further cooling, an incommensurate spin density wave discontinuously develops below $T \approx 150$ K [26]. This might indicate the breakdown of the mean-field approximation deep in the insulating phase where strong electron correlations play a predominant role.

In summary, we have studied the DE model with t_{2g} electrons on the pyrochlore lattice. By taking into account the orbital-dependent hopping, we showed that magnetic properties of spinels close to the metal-insulator transition can be understood by using the picture of cross-linking Kondo chains coupled by localized moments. Our theory provides simple and elegant explanations for the unusual spin superstructure observed in several vanadium spinels. We also proposed a novel noncoplanar tetrahedral order for the magnetic insulating phase of the pyrochlore $Cd_2Os_2O_7$.

We thank Y. Kato, I. Martin, V. Pardo, N. Perkins, and F. Rivadulla for useful discussions. Work at LANL was carried out under the auspices of the U.S. DOE Contract No. DE-AC52-06NA25396 through the LDRD program. G. W. C. is grateful for the hospitality of CNLS at LANL and the support of ICAM and NSF Grant No. DMR-0844115.

[1] M. Imada, A. Fujimori, and Y. Tokura, Rev. Mod. Phys. **70**, 1039 (1998).
[2] H. F. Pen *et al.*, Phys. Rev. Lett. **78**, 1323 (1997).
[3] M. Schmidt *et al.*, Phys. Rev. Lett. **92**, 056402 (2004).
[4] S.-H. Lee *et al.*, Phys. Rev. Lett. **93**, 156407 (2004).
[5] M. Reehuis *et al.*, Eur. Phys. J. B **35**, 311 (2003).
[6] E. M. Wheeler *et al.*, Phys. Rev. B **82**, 140406 (2010).
[7] J. van den Brink and D. Khomskii, Phys. Rev. Lett. **82**, 1016 (1999).
[8] E. Dagotto, *Nanoscale Phase Separation and Colossal Magnetoresistance* (Springer, Berlin, 2003), 1st ed.
[9] D. Ikoma, H. Tsuchiura, and J. Inoue, Phys. Rev. B **68**, 014420 (2003).
[10] A. Ikeda and H. Kawamura, J. Phys. Soc. Jpn. **77**, 073707 (2008).

[11] I. Martin and C. D. Batista, Phys. Rev. Lett. **101**, 156402 (2008).
[12] Y. Akagi and Y. Motome, J. Phys. Soc. Jpn. **79**, 083711 (2010).
[13] Y. Kato, I. Martin, and C. D. Batista, Phys. Rev. Lett. **105**, 266405 (2010).
[14] S. Kumar and J. van den Brink, Phys. Rev. Lett. **105**, 216405 (2010).
[15] Y. Motome and N. Furukawa, Phys. Rev. Lett. **104**, 106407 (2010); J. Phys. Conf. Ser. **200**, 012131 (2010).
[16] G.-W. Chern, Phys. Rev. Lett. **105**, 226403 (2010).
[17] In obtaining $\bar{H}$ we have neglected the Hund's terms that correspond to a hopping of singlet pairs between different orbitals of the same ion.
[18] M. J. P. Gingras, in *Highly Frustrated Magnetism*, edited by C. Lacroix, P. Mendels, and F. Mila (Springer, Berlin, 2011).
[19] H. Tsunetsugu and Y. Motome, Phys. Rev. B **68**, 060405 (R) (2003).
[20] O. Tchernyshyov, Phys. Rev. Lett. **93**, 157206 (2004).
[21] D. I. Khomskii and T. Mizokawa, Phys. Rev. Lett. **94**, 156402 (2005).
[22] V. Pardo *et al.*, Phys. Rev. Lett. **101**, 256403 (2008).
[23] G. Giovannetti *et al.*, Phys. Rev. B **83**, 060402(R) (2011).
[24] A. W. Sleight *et al.*, Solid State Commun. **14**, 357 (1974).
[25] D. Mandrus *et al.*, Phys. Rev. B **63**, 195104 (2001).
[26] A. Koda *et al.*, J. Phys. Soc. Jpn. **76**, 063703 (2007).
[27] T. Tomizawa and H. Kontani, Phys. Rev. B **82**, 104412 (2010).
[28] J. C. Slater and G. F. Koster, Phys. Rev. **94**, 1498 (1954).